JOURNAL OF COMPUTATIONAL PHYSICS **133,** 18–26 (1997)
ARTICLE NO. CP965601

Grid Design for the Computation of a Hexagon-Roll Interaction Using a Finite Element Method

A. C. Skeldon,* K. A. Cliffe,† and D. S. Riley‡

*Department of Mathematics, City University, Northampton Square, London, EC1V 0HB, England; †AEA Technology, B424.4 Harwell, Didcot, Oxon OX11 ORA, England; and ‡Theoretical Mechanics, University Park, Nottingham, NG7 2RD, England
E-mail: a.c.skeldon@city.ac.uk

Received August 23, 1995

Qualitatively incorrect bifurcation diagrams are computed unless the symmetries both of the solutions and of the underlying differential equation are properly accounted for. In the context of the computation of solutions to partial differential equations using the finite element method, this requires careful thought when designing a suitable computational domain and corresponding grid. Here we consider the problem of computing the interaction of hexagon and roll solutions bifurcating from a spatially uniform equilibrium solution of an E(2) equivariant partial differential equation. As an example of where such an interaction occurs we consider a partial differential equation describing the directional solidification of a dilute binary alloy. We show that if the symmetry is not taken into account then spurious disconnections can occur. We describe how to overcome this problem by constructing novel grids which have hexagonal symmetry and enough translational symmetry to enable the computation of the correct bifurcation structure.

1. INTRODUCTION

The domains of partial differential equations modeling real phenomena are often taken to be infinite in order to simplify theoretical analysis. Whilst this leads to many valuable results, there is often a need to perform complimentary numerical computations. These computations have to be carried out on a finite domain, whether it be over a finite spatial domain as in a finite-element method or over a finite frequency range as in spectral methods. The choice of computational domain is influenced strongly by the nature of the expected solutions. For example, the expected solution may be such that coordinate transformations may be used to map the infinite domain to a finite region, or the solution may be periodic allowing the problem to be solved over some finite part of the periodic structure. It is the latter situation that we assume to hold.

Given the periodicity, we still have to decide on the exact choice of domain, what boundary conditions are appropriate, and the way the domain should be discretised. In this paper we address these questions, in the context of the finite element method, for one particular class of bifurcation problems where there is an interaction between two different modes. We indicate a general methodology for grid design using the symmetries of the underlying partial differential equation and of the solutions it is desired to compute.

We assume that the particular solutions of interest are periodic: analysis (e.g. linear stability analysis) of the partial differential equation often indicates the wavenumbers of the solutions on the branches passing through the bifurcation point. A finite domain is chosen which will allow a small number of wavelengths of these solutions; the domain can subsequently be extended by translation and reflection to cover the whole plane. We note that if this is to be done, then only geometries which tile the whole plane can be used; for example, triangles, squares, rectangles, and hexagons.

The original partial differential equation on the infinite domain often has some symmetry: in the case we consider here, the equation is invariant under all rotations, reflections, and translations of the (x, y)-plane, i.e., under the operation of the Euclidean symmetry group, E(2). By imposing boundary conditions, choosing a computational domain, and discretising, we inevitably restrict the symmetry of the computational problem to a subgroup of E(2). This has two effects: first, it limits the solutions which can be computed; and second, because certain disturbances are effectively suppressed by the grid, it may stabilise solutions which would be unstable in the full problem. It is clear that the domain which should be chosen and the way it is discretised depends on the question of primary interest. In our case, the motivation is based on the physical observation that, in a variety of physical systems, both roll and hexagonal solutions are seen and that an exchange of stability between the two can occur. We are therefore interested in designing a grid which can be used to compute the interaction of hexagons and rolls. This kind of modal interaction arises in the well-known Rayleigh–Bénard problem and our methodology is applicable there; the example we present is a model problem in crystal growth. This problem

0021-9991/9797 $25.00

is introduced in Section 2. (We refer to the two-dimensional structures as "rolls" by analogy with the Rayleigh–Bénard problem, although in the context of crystal-growth problems, they might be better described as "bands.")

In Section 3 we show that if proper account of the symmetry is not made, then the bifurcation structure that is computed is qualitatively incorrect. We go on to show how to improve the grid design. The accuracy of the computations carried out on the different grids is compared in Section 4.

2. SOLIDIFICATION PROBLEM

The example considered here arises in the unidirectional solidification of a dilute binary alloy. As the melt is solidified, a boundary forms between the liquid and solid phases. The shape of this interface during the solidification affects the final material properties of the solid and is thus of great industrial significance. If the solidification takes place sufficiently slowly then the interface remains planar, but at greater rates this planar state becomes unstable and both roll and hexagon morphologies are observed. Many simplified models have been constructed to investigate these features: we consider a long-wave equation derived by Brattkus and Davis [1].

Brattkus and Davis' equation is

$$\begin{aligned} H_{\tau\tau} - \nabla^2 H_\tau + \frac{1}{4}(1-\nu^2)\nabla^4 H + \nabla^2 H + \mu^{-1} H \\ = H_\tau \nabla^2 H + |\nabla^2 H|_\tau^2 - \frac{1}{2}(1-\nu)\nabla^2(|\nabla H|^2) \\ - \nu\nabla\cdot(\nabla^2 H \nabla H) - \frac{1}{2}\nabla\cdot(|\nabla H|^2 \nabla H). \end{aligned} \tag{1}$$

It is a partial differential equation describing the evolution with time τ of the interface shape $z = H(x, y, \tau)$ from an initially planar state $z = 0$, where (x, y, z) is a rectangular Cartesian system. It contains two parameters, a scaled "morphological parameter," μ, and a scaled "segregation coefficient," ν. Both μ and ν are strictly positive. Of prime importance for the discussion below is that this partial differential equation is defined over the whole (x, y)-plane and has E(2) symmetry. A consequence of this symmetry is the existence of the trivial solution $H = 0$, in this case representing the planar-interface solution. This is the only solution which has the full symmetry of the equation. Linear analysis shows that, for any given ν, this solution is stable, providing $\mu < \mu_c$, where $\mu_c = 1 - \nu^2$. At μ_c the interface becomes unstable to disturbances of wavenumber k_c given by

$$k_c^2 = \frac{2}{1-\nu^2}.$$

Our initial interest is to compute the branches which bifurcate as μ varies. In spite of the fact that, for $\mu > \mu_c$, the horizontally unbounded planar interface is unstable to a band of wavenumbers about k_c, we consider only the bifurcation structure associated with the critical wave number k_c. The physical justification for this is that although model equations like (1) are defined on the infinite plane, in any real physical situation the domain will be finite. In this case, boundary conditions select out only those solutions that have wavelengths which "fit" in the domain, and solutions with neighbouring wavenumbers are suppressed.

Brattkus and Davis perform a local nonlinear analysis of their equation about $\nu = 1/3$ for three-dimensional hexagonal disturbances. This results in the bifurcation structure presented schematically in Fig. 1. This shows how a measure of the magnitude of the solution (vertical axis, not drawn) changes as the control parameter, μ, is varied. The convention that stable solutions are marked with solid lines whilst unstable solutions are marked with dashed lines is used. Furthermore, where there is more than one bifurcating branch related by symmetry, for simplicity we draw a single branch. For $\mu < \mu_c$ the trivial solution representing the planar interface is stable. At μ_c there is a multi-

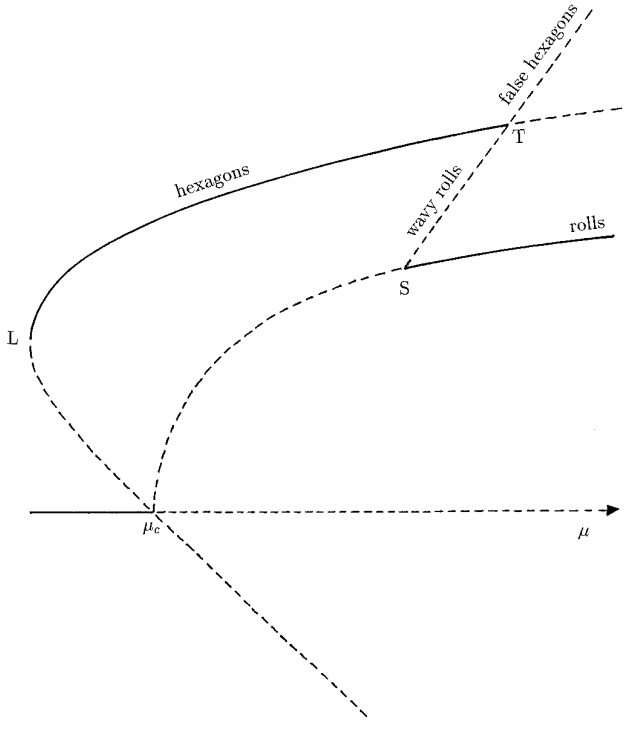

FIG. 1. Schematic bifurcation diagram for the local analysis of Brattkus and Davis' equation. μ_c marks the point where the planar solution becomes unstable, L is a limit point on the hexagonal solution branch, S a symmetry breaking point on the roll branch, and T a transcritical bifurcation point.

ple bifurcation giving rise to both hexagon and roll solutions with the same wave number. In the neighbourhood of μ_c both these solutions are unstable; however, a limit point at L stabilises the branch of hexagons whilst a symmetry-breaking bifurcation at S stabilises the roll solutions. The secondary branch bifurcating from S intersects the hexagonal branch at T in a transcritical bifurcation. This transcritical bifurcation once again destabilises the hexagonal branch.

This bifurcation structure is one of the scenarios which is given by Buzano and Golubitsky [2] who study problems whose solutions are doubly periodic with respect to the hexagonal lattice in the plane. Golubitsky *et al.* [3] consider a similar generic bifurcation problem but with an additional reflection symmetry. This forces the bifurcation to the hexagonal solutions to be a symmetry-breaking bifurcation rather than a transcritical bifurcation. In the case of the Brattkus and Davis equation, this latter situation corresponds to the case $\nu = 1/3$. Knobloch [4] has also considered the local bifurcation structure of a number of long-wavelength convection problems which have a steady-state form similar to Eq. (1). According to his classification, Brattkus and Davis' equation is case B, where $\gamma = 0$ and $\beta \neq \delta$.

Equation (1) is a strongly nonlinear equation: in its derivation it is not assumed that the interface deformation is small. Our original interest was to extend Brattkus and Davis' weakly nonlinear analysis to higher amplitude by the use of numerical path-following and bifurcation methods [5]. This investigation led to the issue of what is an appropriate grid to use to compute the hexagon-roll interaction. It is this question of grid design which is presently discussed: for a fuller discussion to the background to the problem we refer the reader to [5].

In [5] we found that only for values of ν close to 1/3 does the bifurcation structure of Fig. 1 occur at small gradients of the interface. Hence, it is only for ν near 1/3 that we can reliably compute solutions to Eq. (1). For this reason, all the computations presented here were carried out at the fixed value of $\nu = 0.35$.

3. GRID DESIGN FOR THE COMPUTATION OF HEXAGONS AND ROLLS

Roll solutions to (1) may be represented as

$$H_{\text{rolls}}(x, y) = \cos(\mathbf{k_1} \cdot \mathbf{r}),$$

where $\mathbf{k_1}$ is the wave vector associated with the disturbance. Hexagonal solutions result by superimposing three such roll solutions with the same wavelength, but with their wave vectors aligned at 60°. That is,

$$H_{\text{hex}}(x, y) = \cos(\mathbf{k_1} \cdot \mathbf{r}) + \cos(\mathbf{k_2} \cdot \mathbf{r}) + \cos(\mathbf{k_3} \cdot \mathbf{r}),$$

where, without loss of generality,

$$\mathbf{k_1} = k_c(1, 0), \quad \mathbf{k_2} = k_c\left(\frac{1}{2}, \frac{\sqrt{3}}{2}\right), \quad \mathbf{k_3} = k_c\left(-\frac{1}{2}, \frac{\sqrt{3}}{2}\right).$$

Then,

$$H_{\text{hex}}(x, y) = \cos(k_c x) + 2\cos\left(\frac{1}{2}k_c x\right)\cos\left(\frac{\sqrt{3}}{2}k_c y\right),$$

and

$$H_{\text{rolls}}(x, y) = \cos(k_c x). \tag{2}$$

Hence, the rolls have a periodicity of $1/k_c$ in the x-coordinate and are not dependent on y: they appear as rolls lying parallel to the y-axis. In contrast, hexagons have a periodicity of $2/k_c$ in the x-coordinate and of $2/\sqrt{3}k_c$ in the y-coordinate. McFadden *et al.* [6] point out that if a rectangular computational domain of aspect ratio $\sqrt{3}$ is used then both hexagons and rolls solutions "fit" into this domain. Furthermore, if a rectangle of size $2/k_c \times 2/\sqrt{3}k_c$ is used, then each rectangle can contain two x-roll wavelengths or one hexagonal structure. The use of Neumann boundary conditions allows the computation of both hexagons and rolls on a quarter of this domain, that is, on a rectangle of $1/k_c$ by $1/\sqrt{3}k_c$. McFadden *et al.* discretise this domain with rectangular elements and point out that, although the resulting grid does support hexagonal-like solutions, it does not have hexagonal symmetry: for example, the grid is not invariant when it is rotated through 60°. As a consequence, the solutions cannot have exact hexagonal symmetry.

Following McFadden *et al.*, we used a rectangular domain of $1/k_c$ by $1/\sqrt{3}k_c$. A mixed finite element method, similar in nature to the mixed method used to solve the biharmonic equation (see Chapter 7 of [7]) was then implemented. Functions A, B, and C were defined so that

$$A = H_\tau - \nabla^2 H - |\nabla H|^2$$
$$B = \nabla^2 H$$
$$C = |\nabla H|^2,$$

which enabled Eq. (1) to be rewritten in the weak form,

$$\int_D \left\{ \left[\frac{\partial A}{\partial t} + \mu^{-1} H + (1 - A - B - C)B \right] N_1 \right.$$
$$\left. - \left[\frac{1}{4}(1 - \nu^2)\frac{\partial B}{\partial x} + \frac{1}{2}(1 - \nu)\frac{\partial C}{\partial x} + \left(\nu B + \frac{1}{2}C\right)\frac{\partial H}{\partial x} \right] \frac{\partial N_1}{\partial x} \right.$$

$$- \left[\frac{1}{4}(1-\nu^2)\frac{\partial B}{\partial y} + \frac{1}{2}(1-\nu)\frac{\partial C}{\partial y} + \left(\nu B + \frac{1}{2}C\right)\frac{\partial H}{\partial y}\right]\frac{\partial N_1}{\partial y}$$
$$+ \left[\frac{\partial H}{\partial t} - A - B - C\right]N_2 + BN_3 + \frac{\partial H}{\partial x}\frac{\partial N_3}{\partial x} + \frac{\partial H}{\partial y}\frac{\partial N_3}{\partial y}$$
$$+ \left[C - \left(\frac{\partial H}{\partial x}\right)^2 - \left(\frac{\partial H}{\partial y}\right)^2\right]N_4\Bigg\}\,dx\,dy = 0.$$

Here, N_i are the test functions. The test functions are chosen so that these is no contribution from the boundary integral. Note that these equations contain only first derivatives of A, B, C, and H. In our finite-element approximation of these weak equations we expanded A, B, C, and H in quadratic functions. A Galerkin formulation was adopted in which the test functions N_i were chosen from the same set of quadratic basis functions. The resulting integrals were evaluated numerically by Gauss quadrature. The nonlinear algebraic equations for the unknown nodal values of A, B, C, and H were linearized using a Newton–Raphson procedure and the solution of the linear set of equations at each iteration was obtained using a direct frontal solver. Initially the domain was divided into 8×6 nine-noded rectangular elements, though, as discussed below, this was subsequently modified and six-noded triangular elements were used instead.

In order to solve the resulting discretised equation, the software package ENTWIFE, which incorporates extended systems and path-following methods [8], was used. The precise details of this code are not relevant here: the discrepancies between the local analytical results and the computational results, which we discuss below, occur as a result of the lack of symmetry in the discretisation rather than of the numerical algorithmic features of this code. Our results, using the rectangular grid, are presented in the form of a bifurcation diagram in Fig. 2. Here, the vertical axis (not drawn) indicates a measure of the solution, and the bifurcation parameter μ is plotted along the horizontal axis. Whatever the measure chosen to represent the solution, the bifurcation diagram will be qualitatively the same, although with some choices the result can be hard to interpret. In the case presented, we have used the value of the depth to which the interface dips into the solid at the upper left-hand corner of our domain. Computed contour plots of H are drawn for several points along the branches. Note that these contour plots are constructed by reflecting and translating our original computational domain so that the pieces shown consist of 16 copies, i.e., they cover a $4/k_c \times 4/\sqrt{3}k_c$ region of the (x, y)-plane.

At μ_c, in agreement with Brattkus and Davis' local analysis, there is a multiple bifurcation to both roll- and hexagon-like solutions. The solutions on the "hexagonal" branch do not have hexagonal symmetry. This is most readily observed by considering the six triangular regions which surround the central set of concentric circles in each contour plot. If the solutions had hexagonal symmetry, then they would be invariant when rotated through 60°, and hence the separation between the centre of each triangular region and its two neighbours would be the same. On close inspection it is seen that this is not the case. In accordance with the local analysis, the bifurcation to these "hexagons" is transcritical and the solution is initially unstable. These solutions are stabilised at L, which occurs very close to the initial instability. There is a symmetry-breaking bifurcation on the roll branch at S, again in agreement with the local analysis. However, the transcritical bifurcation (T in Fig. 1) has unfolded and in its place are two limit points L_1 and L_2. Consequently, there is a continuous transition from the hexagon-like solutions, which arise at μ_c, to the roll solutions at S.

It might be argued that quantitatively the hexagon-like solutions are close to the true hexagonal solutions of the partial differential equation and that the slight loss of symmetry is not important. However, close to T in Fig. 1, the computed structure is qualitatively incorrect and one of the solution branches becomes disconnected. Path-following methods provide an excellent means of computing solutions to nonlinear problems by systematically working along solution branches, finding bifurcation points, switching to bifurcating branches, and so on. By their very nature, they are not designed to find disconnected branches *ab initio*. It is possible to compute disconnected branches by, for example, switching onto a bifurcated branch and then unfolding the system. Locating disconnected branches about which there is no prior knowledge is, however, a matter of luck. They can be computed by a fortuitous choice of initial guess in the Newton–Raphson procedure, but we know of no systematic means of locating them save for the possibility of introducing unphysical symmetries and regarding the associated bifurcation points of the new problem as organising centres for the physical problem [10]. In the present case, it is only the discrepancy with the local analysis which led us to search for, and find, the disconnected solution branch. In our example, this branch consists of unstable, and therefore physically unrealisable, solutions; but there is no reason why this should always be the case. Hence, not incorporating the symmetry of the solutions in the grid may result in missing important stable solutions: this is no longer an insignificant effect. By returning to the original problem and redesigning our grid, we show how the computed bifurcation structure can be corrected for the example given here, without any increase in the cost of the computations.

The difficulty is that both hexagons and rolls must be computed: if only rolls were required then the rectangular grid used above would create no problems; if only hexagons were required a grid with a hexagonal boundary descretised with equilateral triangles could be used. A hexagonal domain with Neumann or Dirichlet boundary conditions,

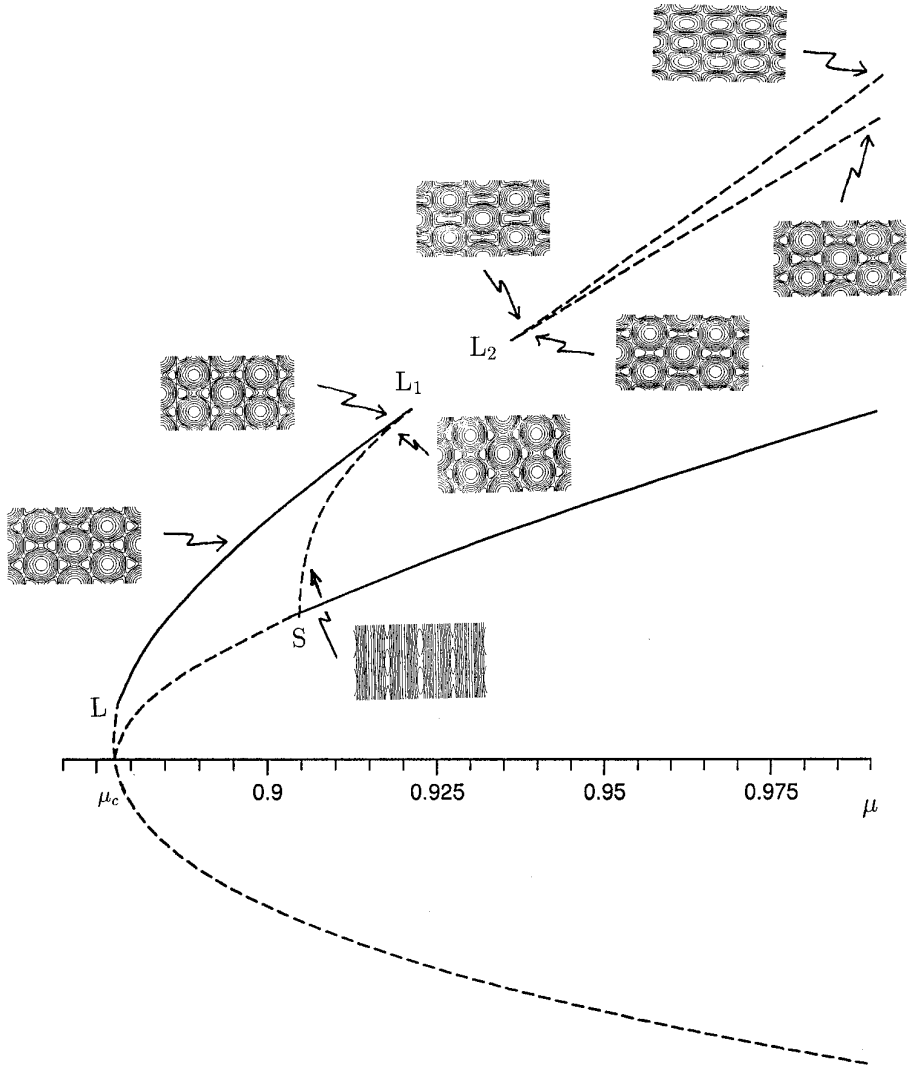

FIG. 2. Computed bifurcation diagram using a rectangular grid of rectangular elements for $\nu = 0.35$ for the Brattkus–Davis equation. At $\mu = 0.8775$ the planar solution becomes unstable. L marks the limit point on the hexagonal solutions branch and S the symmetry breaking bifurcation on the roll branch. L_1 and L_2 are two further limit points. Contour plots of the solutions are shown along some of the branches.

however, cannot support roll solutions. In fact, in order to compute rolls of the form (2), using Neumann or Dirichlet boundary conditions, the computational domain has to be rectangular with sides aligned parallel and perpendicular to the x-axis. Therefore, as in our initial computations, we use a domain with dimensions $1/k_c$ by $1/\sqrt{3}k_c$, so that one roll fits into the rectangle, and once again use Neumann boundary conditions. This domain can be used to tessellate the plane by reflecting in the x-axis and y-axis to produce a template of four rectangles of total size $2/k_c$ by $2/\sqrt{3}k_c$. To tile the entire plane, this template is translated by $(2n/k_c, 2m/\sqrt{3}k_c)$ where $n, m \in \mathbf{Z}$.

In order that the discretised partial differential equation has hexagonal symmetry, the computational domain must be discretised in such a way that when it is used to tessellate the plane it is invariant under the operation of the hexagonal group. Given a point on the plane and an axis through that point, the hexagonal symmetry group is generated by a rotation through 60° (in an anticlockwise direction, say) and a reflection in the axis. Hence we require that the grid is invariant under these same two operations. We have already accepted that the boundary of our computational domain be rectangular (rectangle ACDF in Fig. 3). If we now insist that this grid is invariant under rotations through 60° about A when it is used to tessellate the plane, we generate a number of additional lines as follows: rotating AB through 60° gives the line AE; rotating AF extended through 300° (i.e. $5 \times 60°$) gives AD; rotating FE through 300° gives OB. In order to take account of the reflection symmetry of the hexagonal group, we also require that the

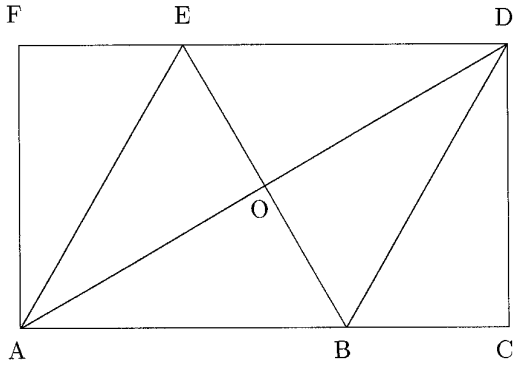

FIG. 3. Invariant lines in a hexagonally symmetric, rectangular grid.

grid is invariant under reflection in one of the invariant lines. For simplicity of description, we choose the axis AD as our reflection axis, although which invariant line is chosen is not important. This is because the equivalent operation to reflection in the other axes through A may be obtained by combinations of reflections in AD and rotations about A. Thus, reflecting OB in AD adds the line OE, and reflecting the line DE in AD results in the line DB. No further lines are generated by rotating any of the given lines in Fig. 3 through 60° about A or by reflecting in the axes AF, AE, AD, and AC that pass through A. Our resulting hexagonally symmetric grid consists of 6 similar triangles. In Fig. 4 we show a region of the plane tessellated as above with this rectangle. The computational grid is marked in bold and this grid rotated through 60° is marked with dashed lines to demonstrate clearly that this nonintuitive grid really does have the rotational symmetry (as well as the reflection symmetry) of the hexagonal group.

The first grid we used for computations consisted of 48 rectangles (8 by 6 elements). A grid with similar resolution may be constructed by dividing each of the six triangles of Fig. 3 into 16 elements. The six triangles are all similar, so, providing all the triangles are discretised in the same way, there is no difficulty in matching nodes along the common sides of the triangles and the hexagonal symmetry is retained. One particular choice is shown in Fig. 5. Computing with the grid shown in Fig. 5 allows the computation of the hexagons correctly: the discretisation no longer allows the continuous deformation from a hexagon to a roll without going through a bifurcation, hence the transcritical bifurcation is not unfolded (see below).

In the original partial differential equation on an infinite domain, a given roll solution is invariant under translations through an integer number of wavelengths. In order to compute the roll solutions correctly the grid must therefore be invariant under translation through the roll wavelength, $1/k_c$. Note that the grid of Fig. 3 does not feature this invariance. Furthermore, rolls bifurcating from the trivial solution break the continuous translational symmetry in the x-coordinate. In order to compute this bifurcation as truly symmetry breaking, rather than transcritical, the grid must contain the symmetry which is broken. No grid can be designed that is invariant under all translations; but we can compromise and insist that the grid is invariant under translation by half of a roll wavelength. This is the simplest choice which includes a symmetry which is broken at the bifurcation to the roll solution, and the bifurcation will therefore be computed correctly. Insisting that the grid is invariant under translations of half of a roll wavelength ($1/2k_c$) also guarantees that our grid will contain the roll

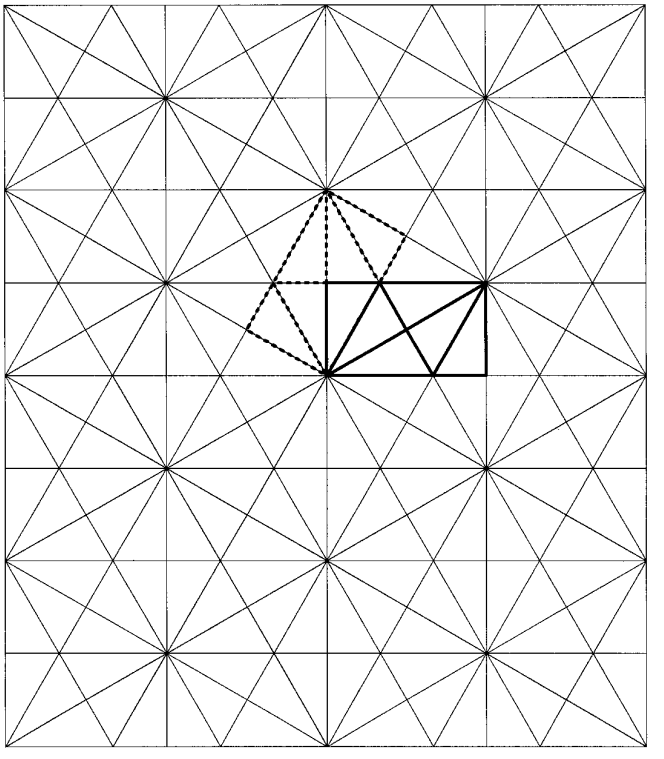

FIG. 4. Region of the plane tessellated with the grid of Fig. 3. The grid of Fig. 3 is shown in bold and the same grid rotated by 60° is shown by the dotted lines.

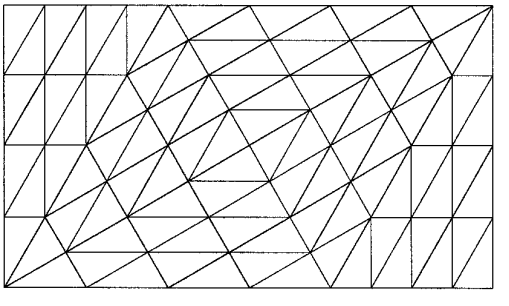

FIG. 5. Grid 3—Hexagonally symmetric rectangular grid of Fig. 3 discretised to give a grid of 96 elements.

symmetry of translation through an integer multiple of wavelengths. Note that in the original partial differential equation, roll solutions of all orientations and all phases are allowed. The alignment of the computational domain allows the computation of only one roll orientation and the boundary conditions select the phase of this solution. Furthermore, true rolls are one-dimensional in nature and have no dependence on the y-coordinate. That is, they are invariant under arbitrary translations in the y-direction. Once again, no grid can possibly have this invariance.

Requiring that the grid of Fig. 3 be invariant when translated through $1/2k_c$ whilst still maintaining the hexagonal invariance results in the 96-element grid of Fig. 6. An interesting point is that this grid consists of 16 rectangles containing scaled down versions of the hexagonally symmetric grid of Fig. 3. The triangles are all similar, so once again a refinement of the grid may be produced by discretising each triangle in an identical way. One example of a 384-element grid where each triangle has been split into 4 is shown in Fig. 7.

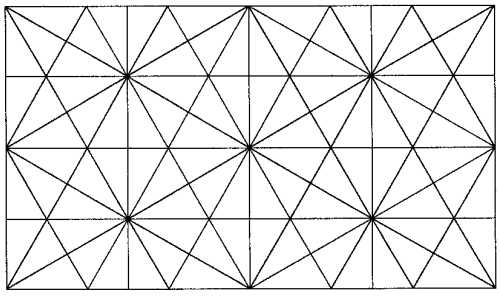

FIG. 6. Grid 4—96 element grid which is both hexagonally symmetric and invariant under translations by $1/2k_c$.

4. RESULTS

It is relatively easy to find whether computation with a given grid results in the disconnection of the transcritical bifurcation or not: if the transcritical bifurcation is disconnected there is a continuous change from hexagon-like solutions to rolls; if not, then there is a bifurcation along the hexagonal solution branch, and the hexagonal solutions themselves may be followed to higher and higher amplitudes. However, to compare the performance of different grids in the computation of the rolls we need to be able to find and identify different types of bifurcation. This follows naturally from the path-following methods incorporated in ENTWIFE which are based on the scheme of Jepson and Spence [8] and the ideas of singularity theory [11]. Under this scheme, each type of bifurcation point has a set of defining conditions. For example, if we wish to find a limit point (a codimension 0 bifurcation) of the set of equations

$$\mathbf{f}(\mathbf{x}, \lambda) = \mathbf{0}, \qquad \mathbf{x} \in \mathbf{X}, \tag{3}$$

where $\mathbf{X}$ is the space of solutions $\mathbf{x}$ and λ is the control parameter, then not only must Eq. (3) be satisfied, but also the defining conditions for the limit point. That is,

$$\mathbf{f}_x(\mathbf{x_0}, \lambda)\boldsymbol{\phi} = \mathbf{0} \tag{4}$$

$$l(\boldsymbol{\phi}) - 1 = 0. \tag{5}$$

Here $\boldsymbol{\phi}$ is the eigenvector of the Jacobian matrix $\mathbf{f}_x(\mathbf{x_0}, \lambda)$ and Eq. (5) is a normalisation of $\boldsymbol{\phi}$. Together, Eqs. (3)–(5) are referred to as an extended system. Whilst this extended system defines necessary conditions for the determination of a limit point, it is not sufficient to exclude the occurrence of all higher codimension bifurcations. In order to rule out these possibilities, ''side constraints'' are also calculated. In the case of the limit point, these are

$$\boldsymbol{\psi}_o \mathbf{f}_{xx} \boldsymbol{\phi}_o \boldsymbol{\phi}_o \tag{6}$$

and

$$\boldsymbol{\psi}_o \mathbf{f}_\lambda, \tag{7}$$

where $\boldsymbol{\psi}_o$ is the left eigenvector of the Jacobian. These expressions must both be nonzero for the bifurcation to be a limit point. If expression (6) is zero, then the bifurcation is either a nondegenerate hysteresis point or an even higher codimension bifurcation point. If expression (7) is zero, then the bifurcation is a transcritical bifurcation point, or again, a higher codimension bifurcation point.

In a similar way, there is an extended system for the computation of a transcritical bifurcation point and two side constraints. In this case, the side constraints monitor whether a bifurcation satisfying the defining conditions is truly transcritical or whether it is a bifurcation of symmetry-breaking or asymmetric-cusp type. Thus, by computing the bifurcation points of Fig. 1 (where possible) and monitoring the corresponding side constraints, the performance of different grids could be evaluated. In each case,

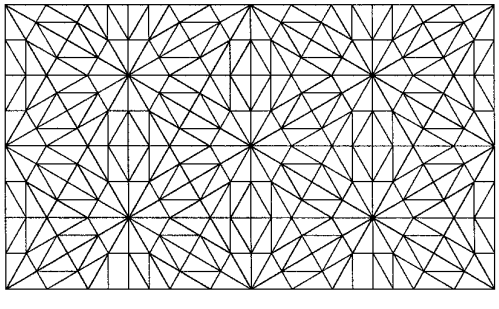

FIG. 7. Grid 5—A refinement of grid 4 producing a 384-element grid.

TABLE I

Computation of the Limit Point on the Connected Hexagonal Solution Branch (L_1 of Fig. 2) Using Grids 1 and 2

			Transcritical Monitor	
Grid	μ	Non-degenerate Hysteresis Monitor	First Parameter	Second Parameter
1	0.91048	-6.87×10^{-2}	-1.97×10^{-2}	5.54×10^{-2}
2	0.92282	-8.57×10^{-3}	-6.07×10^{-3}	2.36×10^{-2}

TABLE III

Computation of the Transcritical Bifurcation on the Hexagonal Solution Branch (T of Fig. 1) Using Grids 3–5

Grid	μ	Pitchfork Monitor	Asymmetric Cusp Monitor
3	0.91738	0.0509	−0.4431
4	0.92623	−0.2538	−10.54
5	0.92748	0.0560	−0.4653

the extended systems were solved using Newton's method, with a convergence criteria such that the norm of the increment made to the solution at the final step is of the order of the machine rounding error. The computations were carried out on the CRAY YMP at the Rutherford Appleton Laboratory.

Five different grids were used as follows:

Grid 1: 8×6 grid of rectangles: 48 rectangular elements.

Grid 2: 16×12 grid of rectangles: 192 rectangular elements.

Grid 3: Hexagonally symmetric grid of 96 triangular elements (Fig. 5).

Grid 4: Hexagonally symmetric grid which is also invariant under translations by $1/2k_c$ (Fig. 6).

Grid 5: Refinement of grid 4; 384 triangular elements (Fig. 7).

As discussed above and illustrated in Fig. 2, the results using grid 1 disagree qualitatively with the local analysis: the transcritical bifurcation point of the local analysis is replaced by two limit points, L_1 and L_2. Refining the rectangular grid and computing with 4 times as many elements (grid 2) does not correct this fundamental problem: there is still a continuous change from the hexagonal solution to the roll solution. Table I lists the values at which the bifurcation L_1 is found and the side constraints (monitors) for the two grids. This same information for L_2 is shown in Table II. The fact that none of the side constraints is zero confirms that the bifurcation points which have been found are limit points and not some higher codimension bifurcation point. The separation of the two limit points is smaller for the finer grid (0.00970 instead of 0.03861), but this does not overcome the problem that the disconnected branch would not normally be found at all using path-following methods. It is well known that if too coarse a discretisation is used, spurious solutions can result; for example, see Murdoch and Budd [9]. Such problems can often be solved in practice by grid refinement. In this case, however, whilst further grid refinement does serve to decrease the separation of the two limit points, it does not eliminate the disconnection.

In contrast, all the grids which contain the hexagonal symmetry (grids 3–5) do not exhibit this unfolding. Instead, in agreement with the local analysis,a transcritical bifurcation point is found (Table III). This is true even for the grids 3 and 4 which have the same number of elements as the coarser of the two rectangular grids. None of the monitors is zero which confirms that the bifurcation is a transcritical bifurcation and not of some higher codimension.

We now turn to the computation of the bifurcations of the roll branch. Table IV shows the results of computing the bifurcation from the trivial solution to the roll solution with the five different grids. This bifurcation is located on the basis that it is a transcritical bifurcation point. The table shows, however, that for all the grids except for grid 3 the pitchfork monitor is zero (to the machine tolerance), that is, using these grids, the bifurcation is given correctly

TABLE II

Computation of the Limit Point on the Disconnected Hexagonal Solution Branch (L_2 of Fig. 2) Using Grids 1 and 2

			Transcritical Monitor	
Grid	μ	Non-degenerate Hysteresis Monitor	First Parameter	Second Parameter
1	0.94909	-1.01×10^{-2}	-3.98×10^{-2}	2.38×10^{-1}
2	0.93252	-9.77×10^{-3}	7.09×10^{-3}	-3.26×10^{-2}

TABLE IV

Computation of the Bifurcation from the Trivial Solution to the Roll Solution

Grid	μ	Pitchfork Monitor
1	0.877500	-1.22×10^{-13}
2	0.877500	-3.81×10^{-12}
3	0.877500	-4.74×10^{-5}
4	0.877500	-6.06×10^{-14}
5	0.877500	-1.94×10^{-12}

TABLE V

Computation of the Symmetry-Breaking Bifurcation on the Roll Branch (S in Fig. 2) Using All Five Grids

Grid	μ	Pitchfork Monitor	Asymmetric Cusp Monitor
1	0.90105	-2.66×10^{-12}	-0.431
2	0.90488	-3.47×10^{-11}	-0.285
3	0.90465	-7.85×10^{-4}	-0.299
4	0.90314	-7.54×10^{-14}	-0.338
5	0.90502	-6.21×10^{-13}	-0.280

as symmetry-breaking. As discussed above, grid 3 does not have the appropriate translational invariance to allow correct computation of the bifurcation to rolls and therefore computes it as a transcritical bifurcation point. This further confirms the need to incorporate the relevant symmetries of the solutions into the grid design.

Table V shows the results of locating the bifurcation on the roll branch to wavy rolls. Once again the pitchfork monitor is zero for all but grid 3, showing that this bifurcation is also symmetry-breaking. The grid 3 calculations give this bifurcation as transcritical, because the grid is not invariant under translations parallel to the y-axis by $1/2\sqrt{3}k_c$. All the other grids do have this translational invariance.

5. CONCLUSION

Although the solutions which are computed without the use of the symmetry may be quantitatively close to the true solutions (the hexagons in our original computations presented in Fig. 2 are close to perfect hexagons), some solutions may not be found at all due to spurious disconnections. In the case presented here the disconnected branch consists of solutions which are unstable and therefore not physically realisable; however, in general, there is no reason why this should be the case. Consequently, physically important solutions may not be accessed by systematic path-following methods, and their computation must rely on "lucky strikes."

Here, we have shown that by using the symmetries of the equations and of the solutions which are to be computed we can design a non-intuitive grid which allows us to produce the qualitatively correct bifurcation diagram for the hexagon-roll interaction. In principle, the underlying message carries over to other numerical schemes such as finite difference methods and finite volume methods: that is, the symmetry of the solutions to be computed should be respected in the discrete equations.

ACKNOWLEDGMENTS

The authors acknowledge the support of the Engineering and Physical Sciences Research Council (GR/K41311) (ACS and DSR) and of the Corporate Research Programme of AEA Technology (KAC).

REFERENCES

1. K. Brattkus and S. H. Davis, *Phys. Rev. B* **38,** 11452 (1988).
2. E. Buzano and M. Golubitsky, *Phil. Trans. R. Soc. London Ser. A* **308,** 617 (1983).
3. M. Golubitsky, J. W. Swift, and E. Knobloch, *Physica D* **10,** 249 (1984).
4. E. Knobloch, *Physica D* **41,** 450 (1990).
5. A. C. Skeldon, G. B. McFadden, M. D. Impey, D. S. Riley, A. A. Wheeler, and S. H. Davis, *Eur. J. App. Math* **6,** 639 (1995).
6. G. B. McFadden, R. F. Boisvert, and S. R. Coriell, *J. Crystal Growth* **84,** 371 (1987).
7. P. G. Ciarlet, "The Finite Element Method for Elliptic Problems," North-Holland, Amsterdam, 1978.
8. A. D. Jepson & A. Spence, *SIAM J. Numer. Anal.* **22,** 736 (1985).
9. T. Murdoch & C. J. Budd, *IMA J. Numer. Anal.* **12,** 365 (1992).
10. D. S. Riley, M. D. Impey & K. H. Winters, *Eur. J. Mech. B/Fluids* **10,** 87 (1991).
11. M. Golubitsky and D. G. Schaeffer, "Singularities and Groups in Bifurcation Theory," Springer Series in Applied Mathematical Sciences, Vol. 51, Springer-Verlag, New York/Berlin, 1984.